Inductively coupled magic angle spinning microresonators benchmarked for high-resolution single embryo metabolomic profiling

Shyam S. Adhikari[a], Li Zhao[b], Thomas Dickmeis[c], Jan G. Korvink[a,], Vlad Badilita[a,]

[a] *Institute of Microstructure Technology (IMT), Karlsruhe Institute of Technology (KIT), Hermann-von-Helmholtz-Platz 1, 76344 Eggenstein-Leopoldshafen, Germany*
[b] *Voxalytic GmbH, Rosengarten 3, 76228, Karlsruhe, Germany*
[c] *Institute of Toxicology and Genetics (ITG), Karlsruhe Institute of Technology (KIT), Hermann-von-Helmholtz-Platz 1, 76344 Eggenstein-Leopoldshafen, Germany.*

†Electronic Supplementary Information

S1. Zebrafish husbandry and embryo culture

Ethics statement: All zebrafish husbandry was performed in accordance with the German animal protection standards and approved by the Government of Baden-Württemberg, Regierungspräsidium Karlsruhe, Germany (Aktenzeichen 35-9185.64/BH KIT).

Adult zebrafish (AB strain) were bred and raised following standard protocols [1]. Briefly, breeding couples were placed into mating tanks in the evening, and eggs were collected from natural spawnings in the morning. Unfertilized eggs were removed, and developing embryos were kept in 10 cm petri dishes (633180, Greiner Bio-One) containing E3 medium [2] without methylene blue at 28 °C. Hatching from the chorions (eggshells) occurred spontaneously 48 hours post fertilization (hpf).

S2. Design and fabrication of the MACS inserts

The fabrication of the microfabricated MACS insert is based on two processes reported previously: the process for the parallel plate capacitor [3] and the process for the wirebonded microcoils [4, 5]. While the performance of the solenoidal microcoils has been well investigated and understood, the on-chip capacitor has proven to be the key element in achieving a high sensitivity MACS insert. Microfabricated inserts introduced by Badilita *et al.* [6] had an interdigitated on-chip capacitor design, with the main advantage of straightforward fabrication: the interdigitated capacitor was fabricated in the same process step as the pads of the wirebonded microcoil in a one-step photolithographic process. However, this interdigitated design is inherently associated with a high series resistance, therefore a low quality factor which ultimately affects the quality factor of the entire MACS microresonator. As an alternative, we have recently introduced a parallel plate design for the on-chip capacitor [3], along with a thorough side-by-side characterization of the two design options. This study has demonstrated an increase in the quality factor of the on-chip capacitor by more than two times, with direct consequence on an improved sensitivity of the MACS microresonator. Moreover, the parallel plate capacitor has shown no significant increase in the sample temperature due to the eddy currents, which also reflects positively in the spectral resolution that can be achieved. The detailed fabrication of the parallel plate capacitor has been presented by Adhikari *et al.* [3].

Thereafter, the fabrication of high aspect ratio SU-8 pillars was carried out using the high viscosity SU-8 2150 photoresist (MicroChem Corp, USA). The hollow SU-8 pillars which act as sample holders and coil support structures were designed with a height of 1300 µm and outer and inner diameter of 850 µm

and 700 µm, respectively. The micro-solenoids were then fabricated using the automated wirebonding process [4, 7]. The particular microresonator reported in this work consists of a micro-solenoid with 13.5 turns, which acts as an inductor connected to the ends of the parallel plate capacitor. The last step of wafer-scale processing was device encapsulation in SU-8 2150, followed by separating each individual device. The final footprint of detectors was 2.85 mm^2, while the inner diameter of the 4 mm MAS rotor is 2.96 mm.

S3. Sample filling and device handling

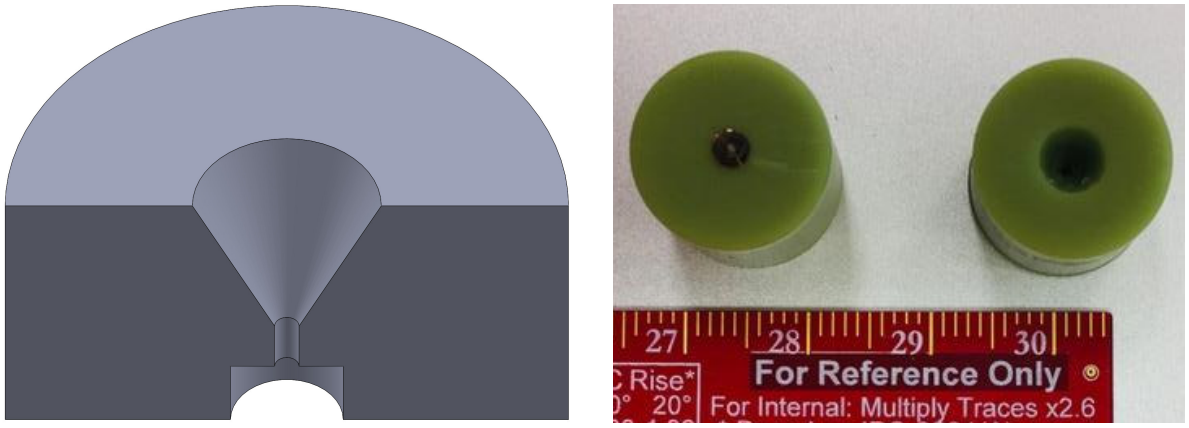

(a) (b)

Figure S1: a) CAD section drawing of a funnel for filling MACS (solids, powders). b) 3D printed funnels.

A sample filling tool was designed and fabricated using a 3D printer (MiiCraft) as shown in the figure S1 to assist in filling powders inside MACS inserts. The bottom part of the tool houses the insert and small channel helps to directly funnel the sample inside the MACS chip. The powder is packed tightly into the MACS device with the help of 400 µm diameter drill bits.

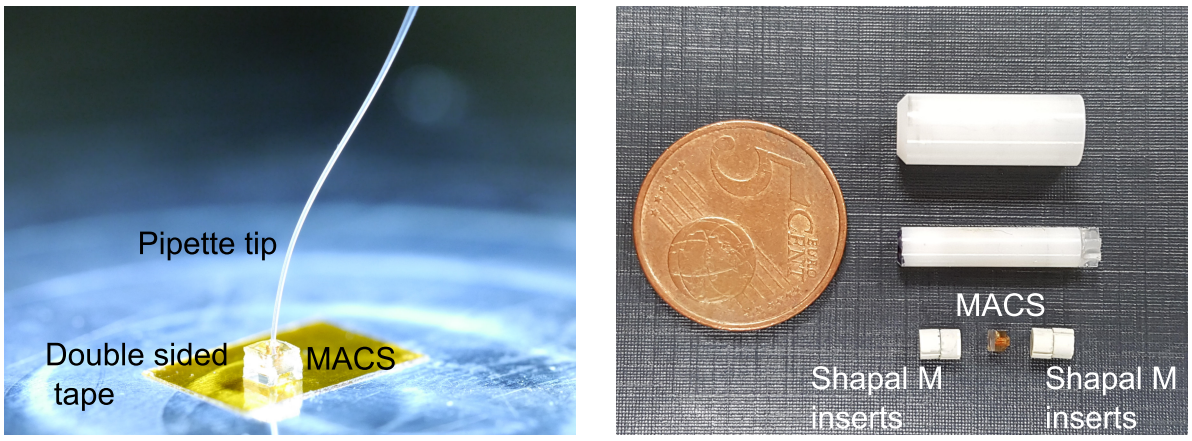

(a) (b)

Figure S2: a) Filling liquid samples inside the MACS insert using an Eppendorf pipette tip. b) MACS inserts are centered with the help of Shapal-M inserts inside the MACS rotor. The Shapal-M inserts also aid in thermal management during NMR experiments.

Liquid samples are dispensed into the MACS devices with the help of a 20 µl Eppendorf pipette and tips (GELoader) under a microscope as shown in figure S2a. The sample region is sealed at the top using a

Biofilm (Applied Biosystems) tape, following which the MACS device is inserted into the MAS rotor with the help of tweezers and centered using Shapal-M inserts (Goodfellow GmbH) as shown in figure S2b.

S4. Sensitivity loss due to off-resonance MACS inserts

Due to the limited range of the tuning and matching capacitors in the MAS probe, MACS resonators in the range of 471 to 529 MHz cannot be used for measurements. This is because after the splitting induced by the coupling of MACS detectors with the coil in the MAS probe, the reflection curve cannot be tuned and matched at 500 MHz. The loss in sensitivity due to this limitation is explained from equation S1 [8].

$$\mathrm{E} = \frac{1}{\sqrt{(1+\frac{k_c}{k})^2 \cdot (1+4\cdot Q_{\mathrm{MACS}}^2 \cdot (\frac{\Delta\omega}{\omega_L})^2)}} \tag{S1}$$

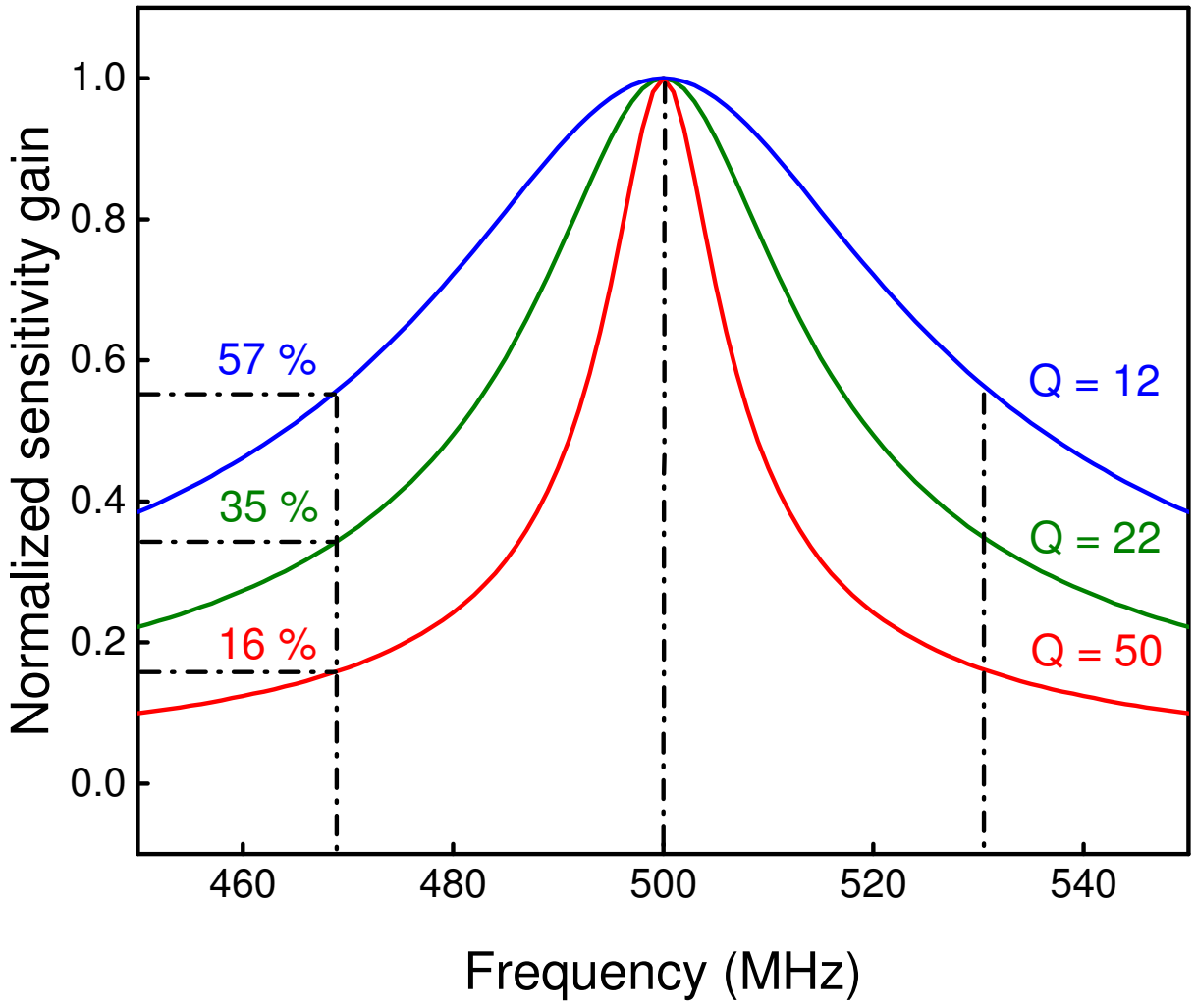

Figure S3: Relative sensitivity gain from MACS with respect to the deviation from the Larmor frequency at various Q factors.

The equation S1 states that any offset ($\Delta\omega$) between the frequency of the MACS insert and the Larmor frequency of interest (ω_L) would lead to a reduction in the sensitivity gain (E) in the MACS arrangement. The equation is derived by calculating the ratio of B_1 field of the respective coils (B_1^{MACS}/B_1^{MAS}) as a function of their Q factors and coupling between them. The MACS efficiency behaviour is plotted in figure S3

for various Q factors at the proton frequency for the current scenario. k_c is the critical coupling between the MACS and MAS coils that can be calculated from their respective Q factor values. The Q value of the MAS solenoid is taken to be 200 [6] and coupling k between the MACS and MAS coils is 0.06.

From figure S3, it is observed that higher the Q of the MACS device, greater the loss in signal enhancement due to inductive coupling. This arises from reduction in bandwidth at higher Q values.

S5. Electrical and thermal characterization

Electrical characterization of the MACS inserts was performed on an RF workbench involving an impedance analyzer (Agilent E4991A) connected to a probe station (Cascade Microtech MPS150) set up with a Z-probe (Z0-20-K3N-GS-500) from Cascade Microtech GmbH. An impedance standard substrate was used to carry out open circuit, closed circuit, and 50 Ω calibration of the Z-probe. The Q factor (shown in figure S4a) and the impedance curve of the resonators were then measured. The resonant frequency of the devices was also verified from the impedance curve.

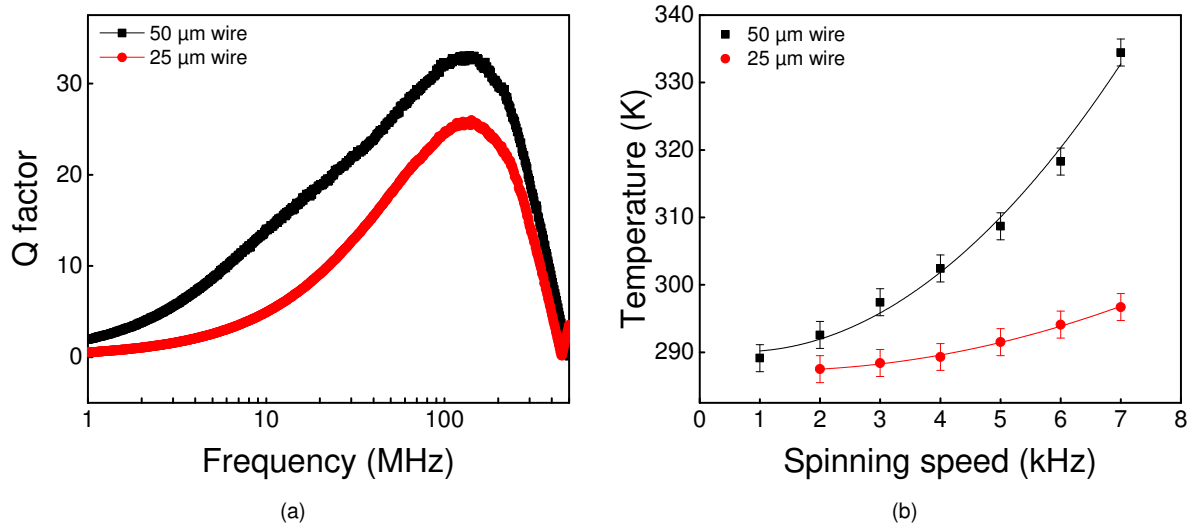

Figure S4: a) Q factor of the MACS devices fabricated with 50 µm and 25 µm insulated copper wire; b) Temperature rise in the sample region of the MACS detectors with 50 µm and 25 µm insulated copper wire. The maximum value of the resonator Q factor moderately increases (from 22 to 32), however the temperature rise is significant when using thicker wire (50 µm) compared to thinner wire (25 µm).

The temperature gradient (shown in figure S4b) inside the MACS inserts at various spinning speeds was determined using the principle of chemical shift thermometry by employing ethylene glycol (Sigma Aldrich) as a reference sample [9]. By observing the frequency difference between the $-OH$ and $-CH_2$ peaks in ethylene glycol at various spinning speeds, the temperature in the sample region of the MACS insert has been calculated. 380 nl of 99 % ethylene glycol was dispensed inside the MACS detector, which was then placed snugly inside an MAS rotor. Shapal-M ceramic spacers [10–12] which are good thermal conductors are used for effective heat transfer from the sample region as well as to center the MACS resonator inside the rotor. The rate of spinning speed was increased from 1 kHz to 7 kHz in steps of 1 kHz and ^1H chemical shift was recorded at each data point. The cooling temperature of the MAS unit was set to 288 K for all experiments.

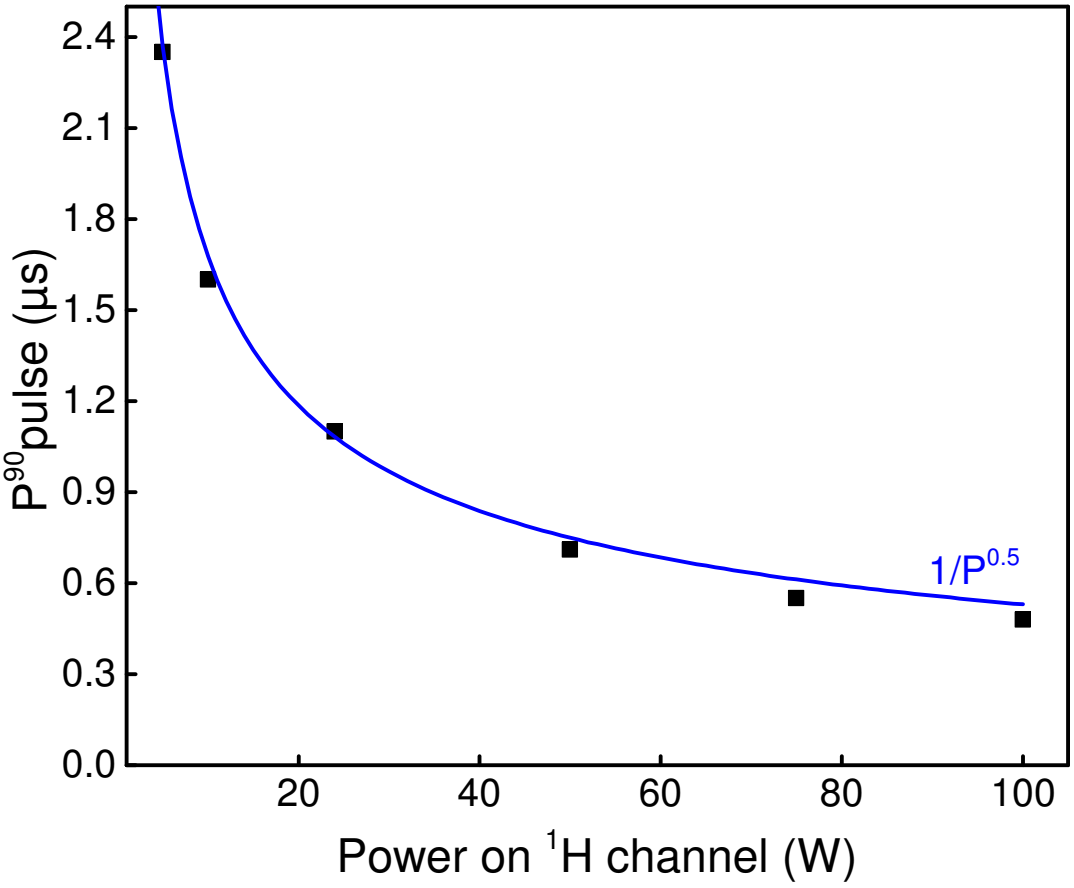

Figure S5: The π/2-pulse length at different excitation power levels on the ^1H channel for the MACS device.

S6. Nutation experiments

Nutation experiments were performed using a sample of adamantane at power levels from 5 W to 100 W on the ^1H channel. The π/2-pulse length was noted down for each power level and numbers are depicted with respect to the power level as shown in the figure S5. The observed deviation at shorter π/2 pulse lengths is due to the shape of the excitation pulse. As the pulse lengths gets shorter, the rise time and fall time (approx. 75 µs each) are in the same order of magnitude as the pulse length itself. The pulse lengths were measured with the help of an oscilloscope. RF nutation frequencies upto 500 kHz was achieved at a power of 100 W on the ^1H channel of the amplifier. However, a few (2 out of 10 tested) MACS devices experienced failure at higher power levels ($\geq$50 W). The failure is attributed to the breakdown of the SU-8 dielectric between the capacitor plates as result of defects during the fabrication process.

S7. COSY experiment calibration

Experiments were performed on 340 mM glucose solution as shown in the figure S6. The acquistion time was 32 min. The solution was prepared by dissolving 67.3 mg of uniformly ^{13}C-labeled glucose (Deutero GmbH) in 1 ml of the D_2O solution. The chemical shifts were reported relative to Trimethylsilyl propionate (TSP) solution. NMR signals were acquired on a Bruker Avance III 500 MHz spectrometer a 4 mm MAS probehead.

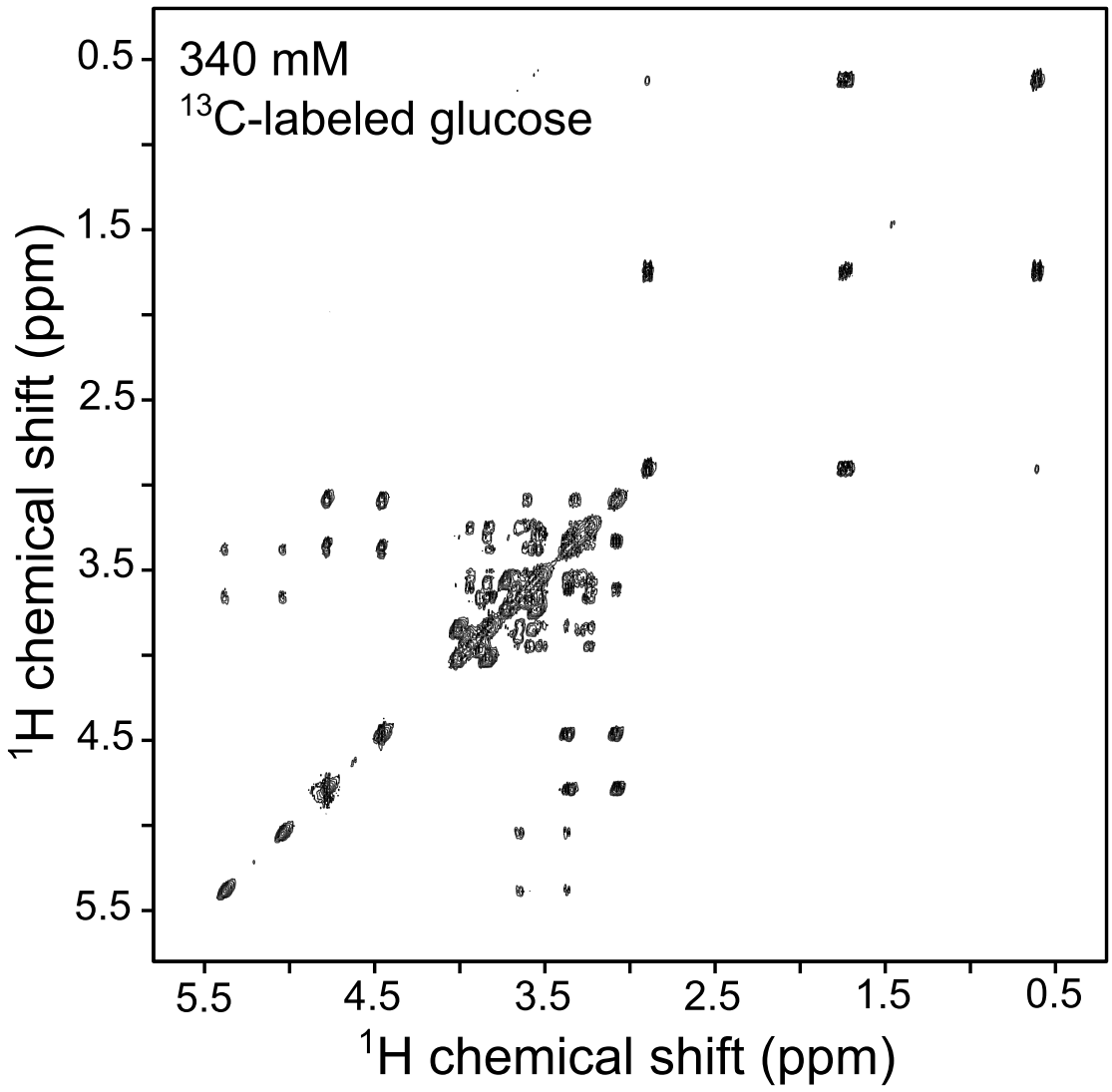

Figure S6: ^{1}H-^{1}H COSY spectrum of 340 mM uniformly ^{13}C-lableled glucose in D_2O obtained using the MACS detector. The total measurement time was 32 min.

S8. Cross Polarization calibration for HMQC experiments

Experiments were performed on 2-^{13}C-labeled glycine sample (Sigma Aldrich). NMR signals were acquired on a Bruker Avance III 500 MHz spectrometer equipped with a 4 mm MAS probehead as shown in figure S7. The ^{1}H-^{13}C decoupling during acquisition was achieved using the WALTZ decoupling scheme with an RF pulse of 100 kHz.

S9. Background signal from SU-8

The background signal that was observed from a blank rotor and SU-8 epoxy which is a constituent part of the MACS device is determined.

A broad peak was observed from SU-8 epoxy between 7-10 ppm as shown in the figure S8. The 4 mm zirconia rotor was filled with around five cylindrical blocks of SU-8 which are 1.5 mm thick and 2.85 mm in diameter and the MAS coil was used for excitation and acquisition. For the control experiment, clean empty zirconia rotors were employed.

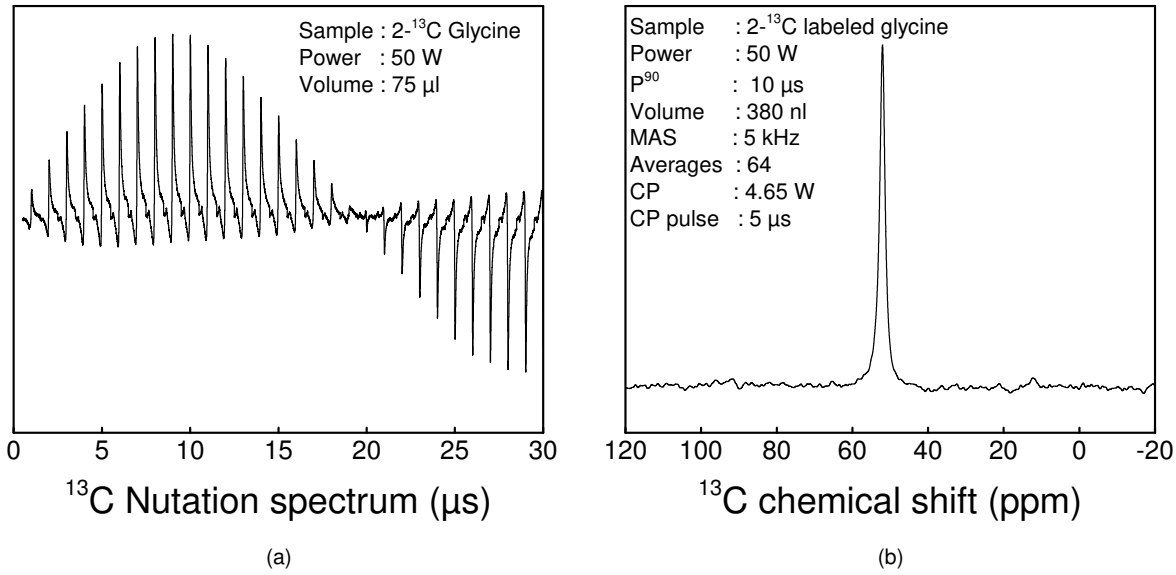

Figure S7: a) Nutation spectrum for the ^{13}C MAS coil at 50 W; b) CP experiment on 2-^{13}C-labeled glycine.

An additional peak was observed in NMR spectrum of the blank rotor which was not present in the spectrum of the rotor with SU-8. This peak is attributed as a ringing artifact from the high Q MAS probe coil which has been isolated as shown in the figure S8b.

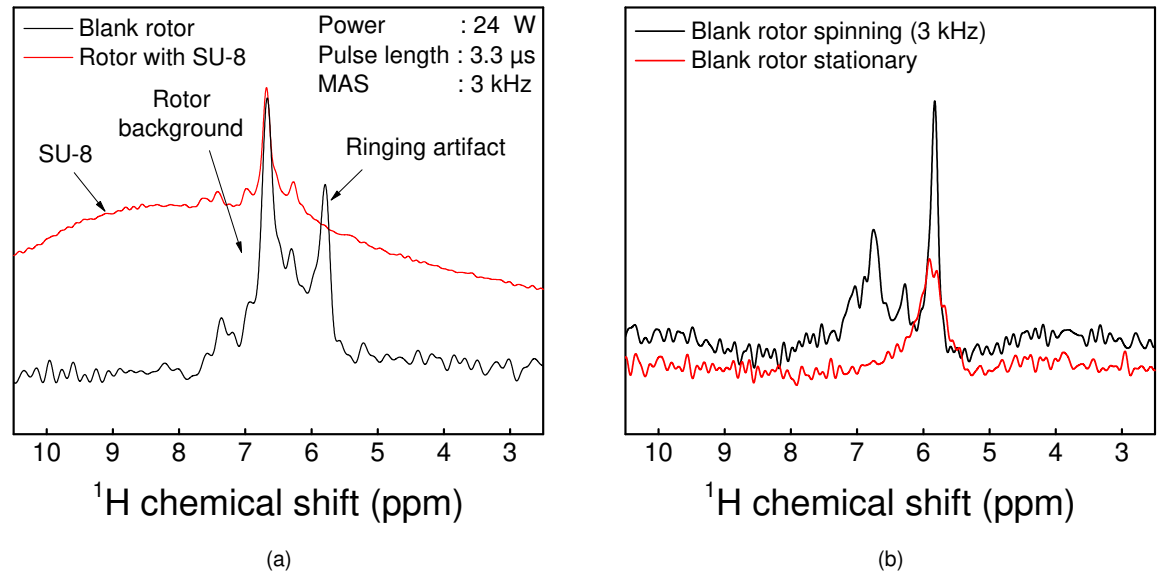

Figure S8: a) SU-8 background spectrum acquired from five cylindrical blocks of SU-8 using the MAS coil for excitation and acquisition; b) Isolating the ringing artifact from the rotor background.

[1] Westerfield Monte. *THE ZEBRAFISH BOOK. A guide for the laboratory use of zebrafish Danio* (Brachydanio) rerio*. University of Oregon Press,Eugene.5 ed. 2007.

[2] Nusslein-Volhard Christiane. *Zebrafish, A Practical Approach*.;261. Oxford University Press, Oxford. 2002.

[3] Adhikari S S., Wallrabe U, Badilita V, Korvink J G.. Capacitor re-design overcomes the rotation rate limit of MACS resonators *Concepts in Magnetic Resonance Part B: Magnetic Resonance Engineering.* 2018;47B:e21362.

[4] Kratt K, Badilita V, Burger T, Korvink J G., Wallrabe U. A fully MEMS-compatible process for 3D high aspect ratio micro coils obtained with an automatic wire bonder *Journal of Micromechanics and Microengineering.* 2010;20:015021.

[5] Badilita V, Kratt K, Baxan N, et al. On-chip three dimensional microcoils for MRI at the microscale *Lab Chip.* 2010;10:1387-1390.

[6] Badilita V, Fassbender B, Kratt K, et al. Microfabricated Inserts for Magic Angle Coil Spinning (MACS) Wireless NMR Spectroscopy *PLoS ONE.* 2012;7:e42848.

[7] Kratt K, Badilita V, Burger T, et al. High aspect ratio PMMA posts and characterization method for micro coils manufactured with an automatic wire bonder *Sensors and Actuators A: Physical.* 2009;156:328 - 333.

[8] Jacquinot J-F, Sakellariou D. NMR signal detection using inductive coupling: Applications to rotating microcoils *Concepts in Magnetic Resonance Part A.* 2011;38A:33–51.

[9] Ammann C, Meier P, Merbach A. A simple multinuclear NMR thermometer *Journal of Magnetic Resonance.* 1982;46:319 - 321.

[10] Sakellariou D, Le Goff G, Jacquinot J-F.. High-resolution, high-sensitivity NMR of nanolitre anisotropic samples by coil spinning *Nature.* 2007;447:694–697.

[11] Inukai M, Takeda K. Double-resonance magic angle coil spinning *Journal of Magnetic Resonance.* 2010;202:274 - 278.

[12] Lehmann-Horn J A., Jacquinot J-F., Ginefri J C., Bonhomme C, Sakellariou D. Monolithic MACS micro resonators *Journal of Magnetic Resonance.* 2016;271:46 - 51.